THE JOURNAL OF PHYSICAL CHEMISTRY LETTERS
A JOURNAL OF THE AMERICAN CHEMICAL SOCIETY

pubs.acs.org/JPCL Letter

Effect of Water Deuteration on Protein Electron Transfer

Setare Mostajabi Sarhangi and Dmitry V. Matyushov*

Cite This: J. Phys. Chem. Lett. 2023, 14, 723–729 Read Online

ACCESS | Metrics & More | Article Recommendations | Supporting Information

ABSTRACT: Traditional theories of long-range protein electron transfer describe the reaction rate in terms of the tunneling distance and the reaction free energy. They do not recognize two physical effects: (i) local wetting of the active site by hydration water and (ii) protein identity affecting the rate through dynamics and flexibility. We find, by molecular dynamics simulations, a significant, ∼25 times, slowing down of the rate of protein electron transfer upon deuteration. H/D substitution changes the rate constant pre-exponential factor in the regime of electron transfer controlled by medium dynamics. Switching from light to heavy water increases the effective medium relaxation time. The effect is caused by both a global change in the flexibility of the protein backbone and locally stronger hydrogen bonds to charged residues.

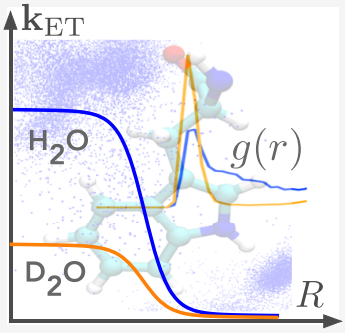

Deuteration of water in chemical kinetics is commonly associated with the kinetic isotope effect (KIE), i.e., the effect of H/D substitution on the reaction rate constant, most commonly applied to H-transfer reactions.[1,2] The results reported here can be classified as solvent KIE[3−5] (caused by the solvent effect) applied to electron transfer: we report significant changes in the rate of protein electron transfer when heavy water, D_2O, replaces the normal water, H_2O, as the solvating medium of the protein. Defining KIE as the ratio of electron-transfer rate constants in H_2O and D_2O, KIE = k_{ET}^{H}/k_{ET}^{D}, we demonstrate here that KIE for protein electron transfer is produced through the effect of deuteration on the rate constant pre-exponential factor $A^{H,D}$:

$$\mathrm{KIE} = A^{H}/A^{D} > 1 \tag{1}$$

The pre-exponential factor is predicted to decrease upon H/D substitution, and the modification of the activation barrier is insignificant.

The textbook explanation of the KIE relates changes in the rate constant to altering frequencies of localized vibrations involving hydrogen atoms upon isotope substitution. Given high frequencies of these vibrations, this is a quantum effect often reduced to a shift of zero-point energy upon deuteration,[6,7] with a corresponding effect on the reaction activation barrier. In contrast, the effect of H/D substitution considered here involves changes in the global dynamics of the protein−water thermal bath affecting the rate pre-exponential factor (eq 1). No modification of the protein itself, due to exchangeable protons, is considered here.

Protein electron transfer is mostly characterized by the rate of long-range electron tunneling and medium reorganization quantified by the medium reorganization energy λ.[8,9] The canonical formulation for λ is Marcus theory[10] operating in terms of electric polarization of the medium. H/D substitution can enter the theory only through changes in the static, ϵ_s, and optical, ϵ_∞, dielectric constants of the medium combined in the Pekar factor $c_0 = \epsilon_\infty^{-1} - \epsilon_s^{-1}$.

The dielectric constants and some dynamic properties of H_2O and D_2O are listed in Table 1. They are compared to corresponding data for two force-field water models used in the simulations described below: TIP3P[11] and TIP3P-HW.[12] Close values of dielectric constants for two water isotopes suggest a very minor effect on the electron-transfer activation barrier. The only noticeable difference in the properties of normal and heavy water belongs to dynamics: heavy water is

Table 1. Physical Properties of H_2O and D_2O at T = 298 K and Physical Properties of Force-Field Water Models (TIP3P and TIP3P-HW)

properties	ϵ_∞	ϵ_s	D^a	η^b	μ^c
H_2O	1.777	78.4	2.30	0.891	1.85
D_2O	1.764	78.1	1.90	1.095	1.87
TIP3P	1.0	94.3[d]	5.48		2.35
TIP3P-HW[12]	1.0		4.25		2.37
TIP3P-HWm	1.0		0.11		2.61

[a]Diffusion constant, $\times 10^{-5}$ cm^2/s. [b]Viscosity, mPa s. [c]Dipole moment in the gas phase, D. [d]From *J. Molec. Phys.***2022**, *364*, 119935.

Received: December 4, 2022
Accepted: January 11, 2023

https://doi.org/10.1021/acs.jpclett.2c03690
J. Phys. Chem. Lett. 2023, 14, 723−729

about 20% slower than normal water when self-diffusion and viscosity are concerned.

Despite no significant difference in dielectric properties required to alter the activation barrier, a number of reports[13−18] have shown a substantial effect of deuteration on the rate of protein electron transfer. An early experimental evidence relevant to our study is the observation by Murgida and Hildebrandt[15] of the H/D effect on the rate of electrochemical protein electron transfer. The rate constant was found to saturate to a plateau with decreasing thickness of the monolayer assembled at the electrode, and it is in that plateau region that the effect of H/D substitution was found. In a different study,[14] intramolecular electron transfer between the active site of azurin and the reduced disulfide bridge linking two cysteine residues showed a weak acceleration of electron transfer in D_2O (inverse KIE): KIE $\simeq$ 0.67. The donor−acceptor (edge-to-edge) distance[19] $\simeq$ 20 Å places this reaction in the nonadiabatic (tunneling[20]) regime, where no significant solvent KIE is anticipated.[15] Consistent with this picture, a more recent study has reported a nearly 300-fold decrease in the conductivity of microbial nanowires composed of polymerized cytochrome OmcS upon deuteration.[18,21] These nanowires are made of cytochrome hemes stacked at 3.5−5 Å edge-to-edge distance[18,22] suggesting that these reactions fall into the plateau region where solvent KIE is expected. A number of protein electron-transfer pathways show similarly short distances between the donor and acceptor sites. For instance, reduction of photoexcited flavin cofactor in cryptochromes and photolyases occurs through chains of 3−4 tryptophan (Trp) cofactors[23] separated by 3.5−4 Å edge-to-edge distance.[24]

The saturation of the electrochemical rate constant in protein-film voltammetry[15,25−28] is related to a long-established dynamical effect of the medium on electron transfer.[29−33] This formulation allows a crossover from an exponential falloff of the rate with the distance to the electrode at larger separations to a saturation plateau at shorter distances, where the rate constant's pre-exponential factor is dictated by the medium dynamics and becomes independent of the protein−electrode separation. An important observation by Murgida and Hildebrandt[15] is that it is only in the dynamics-controlled region of the reaction that one finds a substantial effect of H/D substitution. This observation suggests that diffusive reaction dynamics along the electron-transfer reaction coordinate are affected by deuteration. Molecular dynamics (MD) simulation and theoretical calculations presented in this Letter support this hypothesis. The goal of this study is to establish a physical mechanism, and a theoretical formalism, for a large KIE in protein electron transfer by employing atomistic MD simulations of a realistic system.

Here and elsewhere[34] we use MD simulations to study the activation parameters of transferring a hole from Trp^+ cation radical to Cu^I active site of azurin:[35]

$$(1)\mathrm{Cu^{I}}\text{–}\mathrm{Trp^{+}} \xrightarrow{k_{ET}} \mathrm{Cu^{II}}\text{–}\mathrm{Trp}(2) \tag{2}$$

Here, 1 and 2 mark the initial and final electron-transfer states, respectively. The hole at Trp is initiated by photoexcited Re^I-diimine at the surface of azurin resulting in its fast arrival to the Trp residue.[35] The reaction shown in eq 2 is the rate-limiting step.

MD simulations were set up as described elsewhere[34] and in the Supporting Information (SI). Briefly, azurin protein in two electron-transfer states was solvated with 36469 TIP3P/TIP3P-HW (Table 1) water molecules, and the production simulations of 300 ns were done in the NVT ensemble. TIP3P-HW force field[12] is adopted as the model for D_2O. Additionally, TIP3P-HW force field was slightly modified to increase water's dipole moment by 10%. We found that the self-diffusion constant of bulk water is very sensitive to its dipole moment (Table S1) and used this observation to explore solvation by a significantly slower water model. It turned out that the hydration pattern in the protein pocket around Trp^+ is highly sensitive to the water model as explained below.

The exponential distance falloff of the rate constant is predicted by the nonadiabatic (Marcus−Levich[36]) theory of electron transfer. The nonadiabatic rate constant is proportional to the squared electronic coupling $V(R) \propto \exp[-\gamma R/2]$ and the Boltzmann factor involving the activation barrier $\Delta F^{\dagger}$ required for tunneling resonance (see the SI for more details):

$$k_{NA} \propto V(R)^2 e^{-\beta \Delta F^{\dagger}} \tag{3}$$

where $\beta = (k_B T)^{-1}$. Given that $V(R)$ decays exponentially with the donor−acceptor distance R, one gets an exponential distance decay of the rate constant $k_{NA} \propto V(R)^2 \propto \exp[-\gamma R]$. The overall rate constant of electron transfer includes an additional term[29−33] accounting for the medium dynamics through the dynamical crossover parameter g and takes the form

$$k_{ET} = (1 + g)^{-1} k_{NA} \tag{4}$$

Since $g \propto \tau_X V^2$, one obtains the rate constant scaling as $k_{ET} \propto \tau_X^{-1}$, indicative of overdamped Kramers' kinetics,[37−39] at a sufficiently large electronic coupling V. The relaxation time τ_X is the time of the Stokes-shift dynamics[40] describing relaxation of the donor−acceptor energy gap $X(t)$ viewed as the reaction coordinate for radiationless transitions.[41,42]

The diffusional reaction dynamics for protein−water thermal bath are complex, potentially involving many nuclear degrees of freedom. The most significant nuclear modes affecting the reaction dynamics were identified[43] from the analysis of kinetic data extracted from protein-film electrochemistry.[26,44] These are the energy-gap reaction coordinate $X(t)$ and the donor−acceptor distance $R(t)$. The parameter g in eq 4 follows from mixing the Stokes-shift $[X(t)]$ and distance $[R(t)]$ dynamics:[45]

$$g = \frac{2\pi V^2 \tau_X}{\hbar \sigma_X} \frac{e^{3\gamma^2 \langle (\delta R)^2 \rangle/2}}{\sqrt{2\beta \Delta F^{\dagger} + 4(\tau_X/\tau_R)\gamma^2 \langle (\delta R)^2 \rangle}} \tag{5}$$

Here, $\sigma_X^2 = \langle (\delta X)^2 \rangle = 2\lambda k_B T$ is the variance of the electron-transfer energy gap and $\delta X = X - \langle X \rangle$. All parameters in eq 5, except for γ, depend on the electron-transfer state i = 1, 2; this dependence is dropped for brevity.

The activation barrier entering the Boltzmann factor in the rate constant in eq 3 is the main focus of Marcus theory of electron transfer.[8,9] It is commonly determined through the crossing point of two Marcus parabolas $F_i(X)$, i = 1, 2, given as functions of the energy-gap reaction coordinate.[42,46] However, electron transfer between azurin's active site and Trp creates different wetting patterns[34] in two electron-transfer states, resulting in nonparabolic free-energy surfaces discussed next.

The nonparabolic character of $F_i(X)$ is seen from the fact that the reorganization energies are distinct in two electron-transfer states and different routes to reorganization energies

https://doi.org/10.1021/acs.jpclett.2c03690
J. Phys. Chem. Lett. 2023, 14, 723−729

produce different results (Table 2). The reorganization energy of electron transfer is best defined through the variance of the reaction coordinate in the corresponding state:

$$\lambda_i = \frac{1}{2}\beta\langle(\delta X)^2\rangle_i \tag{6}$$

Two separate reorganization energies λ_i are found (Table 2), which are also different from the Stokes-shift reorganization energy:[47]

$$2\lambda^{St} = X_1 - X_2 \tag{7}$$

Here, $X_i = \langle X\rangle_i$ are two average values of the energy gap calculated from trajectories in equilibrium with the corresponding electron-transfer states $i = 1, 2$. In Marcus theory, all three reorganization energies are equal, $\lambda^{St} = \lambda_1 = \lambda_2$.

The presence of three distinct reorganization energies demands an extension of Marcus crossing parabolas to a theory involving nonparabolic free-energy surfaces. This is accomplished here by applying the Q-model of electron transfer.[46,48] This model stipulates the following inequality between three reorganization energies:

$$\lambda_2 < \lambda^{St} < \lambda_1 \tag{8}$$

where λ_1 and λ_2 can be swapped to match a given reaction. The free-energy surfaces shown in Figure 1 are calculated from λ_i and λ^{St} listed in Table 2 (see the SI) and the experimental reaction free energy[34,35,49] $\Delta F_0 = -0.959$ eV following from the reduction potential of azurin,[50] $E^0 = 0.341$ V, and the reduction potential for the formation of the radical cation Trp^+, $E^0 = 1.3$ V.[49,51] The analytical Q-model is compared to the results of simulations in D_2O (TIP3P-HW, points). The lower portions of the curves are simulation points produced directly from MD. The upper parts of the free-energy surfaces are obtained by shifting the lower sets of points according to the linear relation between the free-energy surfaces[46,52,53] $F_2(X) = F_1(X) + X$ required when Gibbsian ensemble statistics hold.[34,46]

It is clear from both Figure 1 and Table 2 that deuteration does not strongly affect the activation barrier of electron transfer. This is clearly seen from the ratio of nonadiabatic rate constants in normal and deuterated water:

$$KIE_{NA} = k_{NA}^{H}/k_{NA}^{D} = \exp[-\beta\Delta\Delta F^{\dagger}] \tag{9}$$

Table 2. Reorganization Energies (eV) for the Entire System (Azurin and Hydration Water) and for the Protein Component from MD Simulations of Azurin in TIP3P and TIP3P-HW Water at $T = 300$ K[a]

	prot. + TIP3P		protein				
state	λ	λ^{St}	λ	λ^{St}	$\Delta F^{\dagger}$	k_{NA}^{H}/k_{NA}^{D}	k_{ET}^{H}/k_{ET}^{D}
Trp^+-Cu^I	2.09	1.65	2.39	0.82	0.075		
$Trp-Cu^{II}$	1.17		1.28		1.028		
	prot. + TIP3P-HW		protein				
state	λ	λ^{St}	λ	λ^{St}	$\Delta F^{\dagger}$	k_{NA}^{H}/k_{NA}^{D}	k_{ET}^{H}/k_{ET}^{D}
Trp^+-Cu^I	2.50	1.70	3.26	0.85	0.084	0.59	25.0
$Trp-Cu^{II}$	0.98		1.67		1.036	0.37	3.5

[a]Also listed are the activation barriers $\Delta F^{\dagger}$ (eV) and the ratio of the nonadiabatic (NA) and full (ET) rate constants in normal and heavy water.

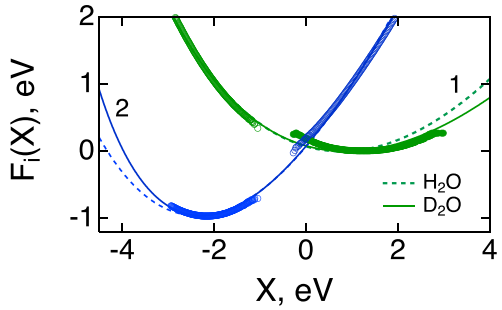

Figure 1. Free-energy surfaces of electron transfer calculated in the Q-model[46,48] (lines, see the SI) and compared to MD simulations in D_2O (points). The calculations are based on λ_i and λ^{St} from MD simulations (Table 2) and the experimental value for the reaction free energy $\Delta F_0 = -0.959$ eV. The dashed lines (Q-model) refer to H_2O, and the solid lines refer to D_2O. The upper portions of the simulation data (D_2O) are obtained from the results around the minima by applying the linear relation $F_2(X) = F_1(X) + X$.

which is fully specified by the change in the activation barrier, $\Delta\Delta F^{\dagger}$. This result is obtained by assuming ΔF_0 not being affected by deuteration (H/D effect on the reduction potential of cytochrome c is about $\simeq$1%[54]). The reduction potential of azurin is 10 mV more positive in D_2O than in H_2O (3% change),[14] which is not sufficient to substantially affect the rate. However, the strongest H/D effect, ~50 mV, on redox potentials is found for redox couples containing aquo ligands,[3] which might be relevant to partially hydrated Trp residue. In addition, since the reduction potential of azurin is pH-dependent,[55,56] corrections for the pH shift upon H/D substitutions are required. Given these uncertainties and reported small shifts of the reduction potential, we have adopted a constant ΔF_0 in the present calculations. We find that deuteration makes the forward rate nearly 25 times slower when quantified by the overall rate constant k_{ET} (Table 2). This change comes from the alteration of the dynamical crossover parameter g in eq 4. The main effect of deuteration on the reaction dynamics is through the reaction pre-exponential factor (eq 1).

The dynamical parameters of the reaction shown in eq 2 are listed in Table 3. They are required to calculate the dynamical crossover parameter g in eq 5. The relaxation times of the energy gap, τ_X, and of the donor–acceptor distance, τ_R, are integral relaxation times calculated from the corresponding time correlation functions (see the SI). The average distance $R_i = \langle R\rangle_i$ is used to calculate the electronic coupling $V = V(R_i)$ in eq 5. Together with the distance variance $\langle(\delta R)^2\rangle_i$ and the activation barrier $\Delta F_i^{\dagger}$ from Table 2, these properties determine the crossover parameters g_i listed in Table 3.

The effect of medium dynamics on the electron-transfer rate becomes essential when $g > 1$ in eq 5. This condition is achieved when the equilibrium donor–acceptor distance $R_i = \langle R\rangle_i$ is shorter than the crossover distance R_i^* determined by the condition $g_i(R_i^*) = 1$. We find $R_1^* = 14.2$ Å and $R_2^* = 10.6$ Å for the reaction in D_2O, which implies $R_1^* > R_1$ and $R_2^* < R_2$ (Table 3). As a result, one finds substantial separations in the values of the crossover parameter $g_1 \gg g_2$ for D_2O in Table 3. Both relaxation times, τ_X and τ_R, contribute to g, and both terms, $\beta\Delta F^{\dagger}$ and $4(\tau_X/\tau_R)\gamma^2\langle(\delta R)^2\rangle$, in the denominator in eq 5 have comparable values. However, the main physical factor

https://doi.org/10.1021/acs.jpclett.2c03690
J. Phys. Chem. Lett. 2023, 14, 723−729

Table 3. Relaxation Times (ps) and Donor−Acceptor Distances for Cu-Trp Charge Transfer (eq 2) as Well as the Crossover Parameter g (eq 5) and the Rate Constants k_{NA} (eq 3) and k_{ET} (eq 4)

state	τ_X	τ_R	$\langle R\rangle$, Å	R^*, Å	$\langle(\delta R)^2\rangle$, Å^2	g	k_{NA}, ns^{-1}	k_{ET}, ns^{-1}
Protein + TIP3P								
Trp^+-Cu^I	44	19	10.3	12.1	0.52	31	11	0.34
$Trp-Cu^{II}$	116	17	9.2	11.2	0.12	50		
Protein + TIP3P-HW								
Trp^+-Cu^I	74	101	10.4	14.2	1.15	1511	19	0.012
$Trp-Cu^{II}$	42	8.5	11.7	10.6	0.07	0.13		

contributing to g_1 in D_2O is a large distance variance in the initial electron-transfer state $\langle(\delta R)^2\rangle_1$ (Figure 2).

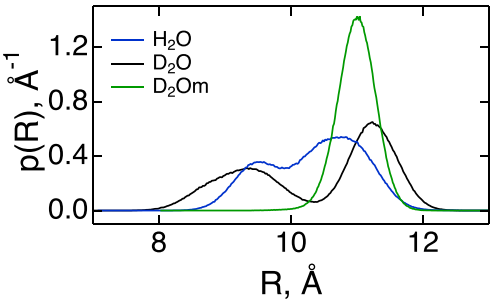

Figure 2. Normalized distribution of donor−acceptor distances R between the Cu atom of the active site of azurin and the indole ring of Trp^+. Calculations are done in the Trp^+-Cu^I (i = 1) state of the protein in H_2O (TIP3P), D_2O (TIP3P-HW), and the modified force field D_2Om (TIP3P-HWm in Table 1).

The standard models for long-range protein electron transfer[57,58] predict reaction rates in terms of the tunneling distance and the reaction free energy (driving force). They do not recognize either the importance of local wetting of the active site by hydration water or the possibility that protein identity can affect the rate through its dynamics and flexibility.[2,59] Both effects turn out to be essential for electron transfer in azurin. The alteration of the local wetting pattern around the Trp residue caused by changing charge distribution (electrowetting, Figure 3) leads to nonparabolic free-energy surfaces of electron transfer with state-dependent reorganization energies (Figure 1). However, this new physics does not predict a noticeable effect of deuteration on the reaction rate within the standard nonadiabatic framework of long-range electron transfer (eq 4): the activation energy is nearly constant upon H/D substitution (eq 9).

It turns out that including medium dynamics is crucial to understand the effect of H/D substitution on electron-transfer kinetics. The transition to the distance-independent Kramers' kinetics[37−39] at $R < R^*$ brings protein identity to the theory of protein electron transfer. The rate constant is now affected by protein flexibility through fluctuations of the donor−acceptor distance and by protein dynamics through the relaxation times τ_X and τ_R. Changing from H_2O to D_2O makes the protein more flexible as quantified by the variance reorganization energies listed in Table 2 and the variance of the donor−acceptor distance in Table 3 (Trp^+-Cu^I state). A strong increase of the distance variance in D_2O compared to H_2O is the main reason for a significantly higher value of the crossover parameter g in D_2O and a corresponding drop of the rate constant (Table 3). Sensitivity of g to the distance variance

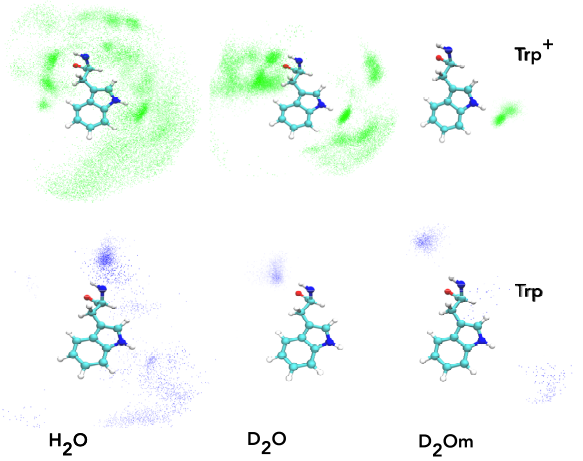

Figure 3. Water density maps within 6 Å cutoff from the center of the indole ring of Trp^+/Trp in TIP3P (left), TIP3P-HW (middle), and TIP3P-HWm (right) water models. The dots in the maps indicate the appearance of water's oxygen atoms within the 6 Å cutoff distance during the last 30 ns of the MD trajectory. The maps are obtained for Trp^+-Cu^I (top row) and $Trp-Cu^{II}$ (bottom row) electron-transfer states.

comes through an exponential term specifying an effective relaxation time in eq 5:

$$\tau_{eff} = \tau_X \exp\left[\frac{3}{2}\gamma^2\langle(\delta R)^2\rangle\right] \quad (10)$$

The hydration pattern seems to be strongly affected by water's identity: the distribution sharply narrows when the modified force field of water, with a 10% higher dipole moment, is used (green line in Figure 2). At the same time, there is no apparent change in the overall number of D_2O compared to H_2O around the indole ring of Trp (Figure S13). Changes in the statistics of the donor−acceptor distance (Figure 2) are caused by local differences in the strength of H-bonds between water and the indole ring of Trp.

Proteins are found to be more compact and globally less flexible in D_2O.[60,61] This is attributed to a stronger hydrophobic effect in D_2O and increased rigidity of the native structure. Structural tightening is also faster than H/D exchange of internal protons, which implies the solvent effect on the protein structure rather than strengthening of intramolecular D-bonds.[61] Our simulations indeed show a tighter structure of D_2O-hydrated azurin in the $Trp-Cu^{II}$ state (Figure 4b). However, the structure becomes more flexible upon H/D substitution for the Trp^+-Cu^I state, as quantified by atomic root-mean-square deviations (rmsd's) of the protein backbone atoms (Figure 4c). This structural softening is

https://doi.org/10.1021/acs.jpclett.2c03690
J. Phys. Chem. Lett. 2023, 14, 723−729

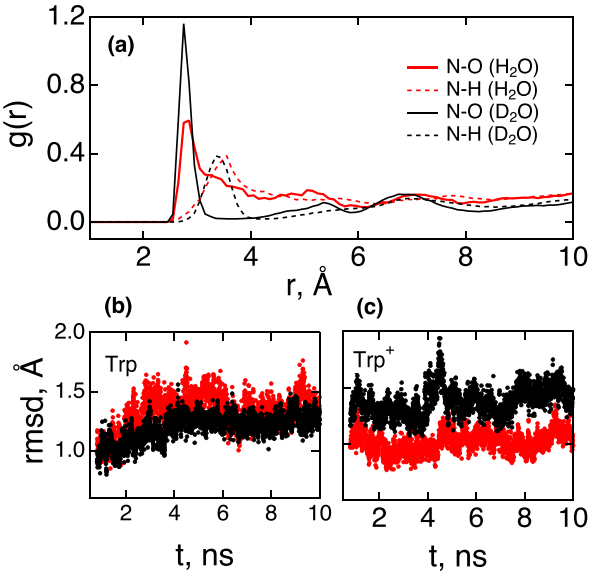

Figure 4. (a) Radial distribution function of oxygens (solid lines) of H_2O (red) and of D_2O (black) around the nitrogen of the indole ring. The dashed line show the distribution functions of water's hydrogens. (b, c) Running averages of the rmsd's of backbone atoms of azurin in H_2O (red) and D_2O (black) in two oxidation states of Trp.

reflected by a broader distribution of electrostatic fluctuations contributing to the free-energy surfaces of electron transfer arising from the protein component of the thermal bath (Figure 5 and Table 2) and in a broader distribution of donor–acceptor distances (Figure 2).

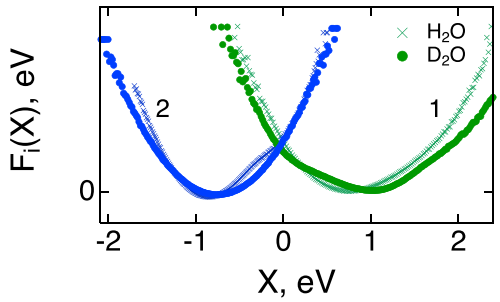

Figure 5. Free-energy surfaces of electron transfer for the protein component of the thermal bath from MD simulations in H_2O (×) and D_2O (●). The free-energy surfaces are plotted with zero reaction free energy and are shifted to cross at $X = 0$.

The reason for changing statistics of the donor–acceptor distance is local. It is promoted by the hydrogen bond between the oxygen atom of hydration water and the hydrogen atom bonded to nitrogen of the indole ring. The D-bond is stronger in heavy water,[62,63] as indicated by the height of the first peak of the pair distribution function shown in Figure 4a. The protons of water are pointing outside (dashed lines in Figure 4a), thus supporting the bonding orientation of water close to the indole ring. Distribution functions of water relative to other atoms of the indole ring (Figures S15 and S16) show larger distances for the first peak and confirm the assignment of the nitrogen atom as the binding site.

The temperature dependence of the KIE[2] predicted by the present model is complex. The variance of the donor–acceptor distance scales linearly with temperature in standard models of harmonic vibrations, but can potentially be complicated by the protein dynamical transition.[64−66] The slope of the dependence $\langle(\delta R)^2\rangle = \chi T$ is substantially increased at the temperature ∼200 K of the dynamical transition, where χ is the inverse force constant (inverse resilience when applied to atomic displacements probed by neutron scattering[65]). The relaxation time changes with temperature according to the Arrhenius law with the activation energy E_τ, and one can anticipate a complex dependence on temperature for the dynamical crossover parameter (eqs 5 and 10):

$$g \propto \exp\left[\frac{E_\tau}{k_B T} + \frac{3}{2}\gamma^2\chi T\right] \tag{11}$$

The crossover from nonadiabatic to dynamics-controlled electron transfer should be accompanied by a change in the Arrhenius slope of the rate constant. To illustrate consequences of $g(T)$, one can calculate the apparent activation enthalpy. Assuming temperature-independent $\Delta F^\dagger$, one obtains[43]

$$\Delta H^\dagger = \Delta F^\dagger + E_\tau - k_B T\gamma^2\langle(\delta R)^2\rangle \tag{12}$$

This equation offers the possibility of a negative apparent activation enthalpy at sufficiently high temperatures and an overall non-Arrhenius dependence of the reaction rate on temperature. Bell-shaped Arrhenius plots were reported for conductivity in OmcS bacterial nanowires.[18,21] The dependence of the reorganization energy and the driving force on temperature, which also contribute to anti-Arrhenius kinetics,[67] can be additionally included. A broad range of temperatures, such as ∼150 K in ref 18 or ∼180 K in ref 67, is required to observe such effects. The combination of a low activation barrier $\Delta F^\dagger$ (Table 2) with a sufficiently large last term in eq 12 allows a weak temperature change of the protein conductivity[68] in a limited range of temperatures. The reaction step studied here (eq 2) is rate-determining in the delivery of charge from the protein surface to the active site,[35] potentially making the entire electron transport weakly affected by temperature.

The main conclusion of this computational study is that there is no clearly distinguishable effect of deuteration on the activation barrier of electron transfer. A substantial effect, ∼25 times slower rate, arises from the effect of deuteration on the dynamics and flexibility of the protein in the regime of dynamically controlled electron transfer. This conclusion is in qualitative agreement with early experiments by Murgida and Hildebrandt.[15] However, the present study does not provide full validations of the large KIE[15,18] reported experimentally given that those data were collected for different proteins (single-heme and multiple-heme cytochromes) and in heterogeneous settings of electrode current measurements. These proteins might alter their dynamics by mechanisms distinct from those found for azurin. The main theoretical principle established here is that protein dynamics and flexibility are affected by H/D substitution leading to a large KIE.

https://doi.org/10.1021/acs.jpclett.2c03690
J. Phys. Chem. Lett. 2023, 14, 723−729

■ ASSOCIATED CONTENT

Data Availability Statement

The data that support the findings are available from the author upon request.

Supporting Information

The Supporting Information is available free of charge at https://pubs.acs.org/doi/10.1021/acs.jpclett.2c03690.

Simulation protocol, additional data, and calculations of the protein dynamics and rates of electron transfer (PDF)

Transparent Peer Review report available (PDF)

■ AUTHOR INFORMATION

Corresponding Author

Dmitry V. Matyushov − *School of Molecular Sciences and Department of Physics, Arizona State University, Tempe, Arizona 85287-1504, United States;* orcid.org/0000-0002-9352-764X; Phone: (480) 965-0057; Email: dmitrym@asu.edu

Author

Setare Mostajabi Sarhangi − *School of Molecular Sciences and Department of Physics, Arizona State University, Tempe, Arizona 85287-1504, United States*

Complete contact information is available at: https://pubs.acs.org/10.1021/acs.jpclett.2c03690

Notes

The authors declare no competing financial interest.

■ ACKNOWLEDGMENTS

This research was supported by the Army Research Office (ARO-W911NF2010320) and by the National Science Foundation (CHE-2154465). The supercomputer time was provided through Extreme Science and Engineering Discovery Environment (XSEDE) allocation MCB080071 and through ASU's Research Computing. Inspiring discussions with Stuart Lindsay are gratefully acknowledged.

■ REFERENCES

(1) Kohen, A., Limbach, H.-H., Eds. *Isotope Effect in Chemistry and Biology*; CRC Press: Boca Raton, 2006.

(2) Klinman, J. P.; Kohen, A. Hydrogen tunneling links protein dynamics to enzyme catalysis. *Annu. Rev. Biochem.* **2013**, *82*, 471−496.

(3) Weaver, M. J.; Nettles, S. M. Solvent isotope effects upon the thermodynamics of some transition-metal redox couples in aqueous media. *Inorg. Chem.* **1980**, *19*, 1641−1646.

(4) Makhatadze, G. I.; Clore, G. M.; Gronenborn, A. M. Solvent isotope effect and protein stability. *Nat. Struct. Biol.* **1995**, *2*, 852−855.

(5) Quinn, D. M. In *Isotope Effects in Chemistry and Biology*; Kohen, A., Limbach, H.-H., Eds.; CRC Press: Boca Raton, 2006; Chapter 41, pp 995−1018.

(6) Nagel, Z. D.; Klinman, J. P. Tunneling and dynamics in enzymatic hydride transfer. *Chem. Rev.* **2006**, *106*, 3095−3118.

(7) Sen, A.; Kohen, A. Enzymatic tunneling and kinetic isotope effects: chemistry at the crossroads. *J. Phys. Org. Chem.* **2010**, *23*, 613−619.

(8) Marcus, R. A.; Sutin, N. Electron transfer in chemistry and biology. *Biochim. Biophys. Acta* **1985**, *811*, 265−322.

(9) Nitzan, A.*Chemical Dynamics in Condensed Phases: Relaxation, Transfer and Reactions in Condensed Molecular Systems*; Oxford University Press: Oxford, 2006.

(10) Marcus, R. A. Electrostatic free energy and other properties of states having nonequilibrium polarization. I. *J. Chem. Phys.* **1956**, *24*, 979−989.

(11) Jorgensen, W. L.; Chandrasekhar, J.; Madura, J. D.; Impey, R. W.; Klein, M. L. Comparison of simple potential functions for simulating liquid water. *J. Chem. Phys.* **1983**, *79*, 926−935.

(12) Linse, J.-B.; Hub, J. S. Three- and four-site models for heavy water: SPC/E-HW, TIP3P-HW, and TIP4P/2005-HW. *J. Chem. Phys.* **2021**, *154*, 194501.

(13) Hille, R. Electron transfer within xanthine oxidase: a solvent kinetic isotope effect study. *Biochemistry* **1991**, *30*, 8522−8529.

(14) Farver, O.; Zhang, J.; Chi, Q.; Pecht, I.; Ulstrup, J. Deuterium isotope effect on the intramolecular electron transfer in Pseudomonas aeruginosa azurin. *Proc. Natl. Acad. Sci. U.S.A.* **2001**, *98*, 4426−4430.

(15) Murgida, D. H.; Hildebrandt, P. Proton-coupled electron transfer of cytochrome c. *J. Am. Chem. Soc.* **2001**, *123*, 4062−4068.

(16) Byrdin, M.; Sartor, V.; Eker, A. P.; Vos, M. H.; Aubert, C.; Brettel, K.; Mathis, P. Intraprotein electron transfer and proton dynamics during photoactivation of DNA photolyase from E. coli: review and new insights from an "inverse" deuterium isotope effect. *Biochimica et Biophysica Acta (BBA) - Bioenergetics* **2004**, *1655*, 64−70.

(17) Amdursky, N.; Pecht, I.; Sheves, M.; Cahen, D. Marked changes in electron transport through the blue copper protein azurin in the solid state upon deuteration. *Proc. Natl. Acad. Sci. U.S.A.* **2013**, *110*, 507−512.

(18) Dahl, P. J.; Yi, S. M.; Gu, Y.; Acharya, A.; Shipps, C.; Neu, J.; O'Brien, J. P.; Morzan, U. N.; Chaudhuri, S.; Guberman-Pfeffer, M. J.; et al. A 300-fold conductivity increase in microbial cytochrome nanowires due to temperature-induced restructuring of hydrogen bonding networks. *Sci. Adv.* **2022**, *8*, eabm7193.

(19) Farver, O.; Pecht, I. Long-range intramolecular electron transfer in azurins. *Proc. Natl. Acad. Sci. U.S.A.* **1989**, *86*, 6968−6972.

(20) DeVault, D.*Quantum-Mechanical Tunneling in Biologycal Systems*; Cambridge University Press: Cambridge, UK, 1984.

(21) Guberman-Pfeffer, M. J. Assessing thermal response of redox conduction for nti-Arrhenius kinetics in a microbial cytochrome nanowire. *J. Phys. Chem. B* **2022**, *126*, 10083−10097.

(22) Yalcin, S. E.; Malvankar, N. S. The blind men and the filament: Understanding structures and functions of microbial nanowires. *Cur. Opin. Chem. Biol.* **2020**, *59*, 193−201.

(23) Müller, P.; Yamamoto, J.; Martin, R.; Iwai, S.; Brettel, K. Discovery and functional analysis of a 4th electron-transferring tryptophan conserved exclusively in animal cryptochromes and (6−4) photolyases. *Chem. Commun.* **2015**, *51*, 15502−15505.

(24) Cailliez, F.; Müller, P.; Firmino, T.; Pernot, P.; de la Lande, A. Energetics of photoinduced charge migration within the tryptophan tetrad of an animal (6−4) photolyase. *J. Am. Chem. Soc.* **2016**, *138*, 1904−1915.

(25) Murgida, D. H.; Hildebrandt, P. Redox and redox-coupled processes of heme proteins and enzymes at electrochemical interfaces. *Phys. Chem. Chem. Phys.* **2005**, *7*, 3773−3784.

(26) Waldeck, D. H.; Khoshtariya, D. E.*Applications of Electrochemistry and Nanotechnology in Biology and Medicine I*; Springer: New York, 2011; pp 105−238.

(27) Alvarez-Paggi, D.; Hannibal, L.; Castro, M. A.; Oviedo-Rouco, S.; Demicheli, V.; Tórtora, V.; Tomasina, F.; Radi, R.; Murgida, D. H. Multifunctional cytochrome c: Learning new tricks from an old dog. *Chem. Rev.* **2017**, *117*, 13382−13460.

(28) Buhrke, D.; Hildebrandt, P. Probing structure and reaction dynamics of proteins using time-resolved resonance Raman spectroscopy. *Chem. Rev.* **2020**, *120*, 3577−3630.

(29) Zusman, L. D. Outer-sphere electron transfer in polar solvents. *Chem. Phys.* **1980**, *49*, 295−304.

(30) Sumi, H.; Marcus, R. A. Dynamical effects in electron transfer reactions. *J. Chem. Phys.* **1986**, *84*, 4894−4914.

(31) Hynes, J. T. Outer-sphere electron-transfer reactions and frequency-dependent friction. *J. Phys. Chem.* **1986**, *90*, 3701−3706.

(32) Rips, I.; Jortner, J. Dynamic solvent effects on outer-sphere electron transfer. *J. Chem. Phys.* **1987**, *87*, 2090−2104.
(33) Yan, Y. J.; Sparpaglione, M.; Mukamel, S. Solvation dynamics in electron-transfer, isomerization, and nonlinear optical processes: a unified Liouville-space theory. *J. Phys. Chem.* **1988**, *92*, 4842−4853.
(34) Sarhangi, S. M.; Matyushov, D. V. Theory of protein charge transfer: Electron transfer between tryptophan residue and active site of azurin. *J. Phys. Chem. B* **2022**, *126*, 10360.
(35) Shih, C.; Museth, A. K.; Abrahamsson, M.; Blanco-Rodriguez, A. M.; Bilio, A. J. D.; Sudhamsu, J.; Crane, B. R.; Ronayne, K. L.; Towrie, M.; Vlček, A.; et al. Tryptophan-accelerated electron flow through proteins. *Science* **2008**, *320*, 1760−1762.
(36) Levich, V. G. In *Advances in Electrochemistry and Electrochemical Engineering*; Delahay, P., Ed.; Interscience: New York, 1965; Vol. 4, pp 1−124.
(37) Kramers, H. Brownian motion in a field of force and the diffusion model of chemical reactions. *Physica* **1940**, *7*, 284−304.
(38) Frauenfelder, H.; Wolynes, P. G. Rate theories and puzzles of hemeprotein kinetics. *Science* **1985**, *229*, 337−345.
(39) Hänggi, P.; Talkner, P.; Borkovec, M. Reaction-rate theory: fifty years after Kramers. *Rev. Mod. Phys.* **1990**, *62*, 251−341.
(40) Maroncelli, M. The dynamics of solvation in polar liquids. *J. Mol. Liq.* **1993**, *57*, 1−37.
(41) Lax, M. The Frank-Condon principle and its application to crystals. *J. Chem. Phys.* **1952**, *20*, 1752−1760.
(42) Warshel, A. Dynamics of reactions in polar solvents. Semiclassical trajectory studies of electron-transfer and proton-transfer reactions. *J. Phys. Chem.* **1982**, *86*, 2218−2224.
(43) Matyushov, D. V. Dynamical effects in protein electrochemistry. *J. Phys. Chem. B* **2019**, *123*, 7290−7301.
(44) Zitare, U. A.; Szuster, J.; Santalla, M. C.; Morgada, M. N.; Vila, A. J.; Murgida, D. H. Dynamical effects in metalloprotein heterogeneous electron transfer. *Electrochim. Acta* **2020**, *342*, 136095.
(45) Matyushov, D. V. Conformational dynamics modulating electron transfer. *J. Chem. Phys.* **2022**, *157*, 095102.
(46) Small, D. W.; Matyushov, D. V.; Voth, G. A. The theory of electron transfer: What may be missing? *J. Am. Chem. Soc.* **2003**, *125*, 7470−7478.
(47) LeBard, D. N.; Matyushov, D. V. Protein-water electrostatics and principles of bioenergetics. *Phys. Chem. Chem. Phys.* **2010**, *12*, 15335−15348.
(48) Matyushov, D. V.; Voth, G. A. Modeling the free energy surfaces of electron transfer in condensed phases. *J. Chem. Phys.* **2000**, *113*, 5413.
(49) Gray, H. B.; Winkler, J. R. Functional and protective hole hopping in metalloenzymes. *Chem. Sci.* **2021**, *12*, 13988−14003.
(50) Garner, D. K.; Vaughan, M. D.; Hwang, H. J.; Savelieff, M. G.; Berry, S. M.; Honek, J. F.; Lu, Y. Reduction potential tuning of the blue copper center in Pseudomonas Aeruginosa azurin by the axial methionine as probed by unnatural amino acids. *J. Am. Chem. Soc.* **2006**, *128*, 15608−15617.
(51) Glover, S. D.; Tyburski, R.; Liang, L.; Tommos, C.; Hammarström, L. Pourbaix diagram, proton-coupled electron transfer, and decay kinetics of a protein tryptophan radical: Comparing the redox properties of W32 * and Y32 * generated inside the structurally characterized α_3W and α_3Y proteins. *J. Am. Chem. Soc.* **2018**, *140*, 185−192.
(52) Bennett, C. H. Efficient estimation of free energy differences from Monte Carlo data. *J. Comput. Phys.* **1976**, *22*, 245−268.
(53) Tachiya, M. Relation between the electron-transfer rate and the free energy change of reaction. *J. Phys. Chem.* **1989**, *93*, 7050−7052.
(54) Battistuzzi, G.; Borsari, M.; Ranieri, A.; Sola, M. Solvent-based deuterium isotope effects on the redox thermodynamics of cytochrome c. *J. Biol. Inorg. Chem.* **2004**, *9*, 781−787.
(55) St. Clair, C. S.; Ellis, W. R.; Gray, H. B. Spectroelectrochemistry of blue copper proteins: pH and temperature dependences of the reduction potentials of five azurins. *Inorg. Chim. Acta* **1992**, *191*, 149−155.
(56) Tyson, K. J.; Davis, A. N.; Norris, J. L.; Bartolotti, L. J.; Hvastkovs, E. G.; Offenbacher, A. R. Impact of local electrostatics on the redox properties of tryptophan radicals in azurin: Implications for redox-active tryptophans in proton-coupled electron transfer. *J. Phys. Chem. Lett.* **2020**, *11*, 2408−2413.
(57) Page, C. C.; Moser, C. C.; Chen, X. X.; Dutton, P. L. Natural engineering principles of electron tunneling in biological oxidation-reduction. *Nature* **1999**, *402*, 47−52.
(58) Gray, H. B.; Winkler, J. R. Long-range electron transfer. *Proc. Natl. Acad. Sci. U. S. A.* **2005**, *102*, 3534−3539.
(59) Eisenmesser, E. Z.; Millet, O.; Labeikovsky, W.; Korzhnev, D. M.; Wolf-Watz, M.; Bosco, D. A.; Skalicky, J. J.; Kay, L. E.; Kern, D. Intrinsic dynamics of an enzyme underlies catalysis. *Nature* **2005**, *438*, 117−121.
(60) Jasnin, M.; Tehei, M.; Moulin, M.; Haertlein, M.; Zaccai, G. Solvent isotope effect on macromolecular dynamics in E. coli. *Eur. Biophys J.* **2008**, *37*, 613−617.
(61) Cioni, P.; Strambini, G. B. Effect of heavy water on protein flexibility. *Biophys. J.* **2002**, *82*, 3246−3253.
(62) Likhodi, O.; Chalikian, T. V. Differential hydration of α,ω-aminocarboxylic acids in D2O and H2O. *J. Am. Chem. Soc.* **2000**, *122*, 7860−7868.
(63) Scheiner, S.; Čuma, M. Relative stability of hydrogen and deuterium bonds. *J. Am. Chem. Soc.* **1996**, *118*, 1511−1521.
(64) Parak, F. G. Physical aspects of protein dynamics. *Rep. Prog. Phys.* **2003**, *66*, 103−129.
(65) Zaccai, G. How soft is a protein? A protein dynamics force constant measured by neutron scattering. *Science* **2000**, *288*, 1604−1607.
(66) Doster, W. The protein-solvent glass transition. *Biochim. Biophys. Acta* **2010**, *1804*, 3−14.
(67) Waskasi, M. M.; Kodis, G.; Moore, A. L.; Moore, T. A.; Gust, D.; Matyushov, D. V. Marcus bell-shaped electron transfer kinetics observed in an Arrhenius plot. *J. Am. Chem. Soc.* **2016**, *138*, 9251−9257.
(68) Amdursky, N.; Sepunaru, L.; Raichlin, S.; Pecht, I.; Sheves, M.; Cahen, D. Electron transfer proteins as electronic conductors: Significance of the metal and its binding site in the blue Cu protein, azurin. *Adv. Sci.* **2015**, *2*, 1400026.

https://doi.org/10.1021/acs.jpclett.2c03690
J. Phys. Chem. Lett. 2023, 14, 723−729